

Check for updates

Boosting Electrochemical Urea Synthesis via Cooperative Electroreduction Through the Parallel Reduction

Yalan Zhang, Jie Hu, Huike Zhou, Yingpeng Zhang, Zebin Yu, Qiang Wei, Wenrong Xiong, Lijun Chen, Zhifei Yu, Jiahao Yang, Wei Liu, Hu Du, Jinying Xu, Sunlin Chi, Aiying Wang, and Xianchuan Xie*

Despite recent achievements in the co-reduction electrosynthesis of urea from nitrogen wastes and CO2, the selectivity and yield of the products remain fairly average because of the competition of the NITRR, CO₂RR, and HER. Here, a strategy involving FeNC catalysts disperse with oxygen-vacancy-rich CeO₂ (FeNC-Ce) is illustrated, in which the reversible hydrogenation of defects, and bimetallic catalytic centers enable spontaneous switching between the reduction paths of NO₃⁻ and CO₂. The FeNC-Ce electrocatalyst exhibits an extremely high urea yield and Faraday efficiency (FE) of 20969.2 μg mg⁻¹ h⁻¹ and 89.3%, respectively, which is highly superior to most reported values (maximum urea yield of 200–2300 μ g mg⁻¹ h⁻¹, FE_{max} of 11.5%–83.4%). The study findings, rationalize by in situ spectroscopy and theoretical calculations, are rooted in the evolution of dynamic NITRR and CO2RR co-reduction involving protons, alleviating the overwhelming single-system reduction of reactants and thereby minimizing the formation of by-products.

Y. Zhang, J. Hu, H. Zhou, W. Xiong, L. Chen, Z. Yu, J. Yang, W. Liu, H. Du, J. Xu, S. Chi, X. Xie

Key Laboratory of Poyang Lake Environment and Resource Utilization Engineering Research Center of Watershed Carbon Neutralization Ministry of Education

School of Resource and Environment

Nanchang University Nanchang 330031, China

E-mail: xchxie@ncu.edu.cn

School of Materials and Chemical Engineering Ningbo University of Technology

Ningbo 315211, China

Z. Yu

School of Resources

Environment and Materials

Guangxi University

Nanning 530004, P. R. China

CAS Key Laboratory of Urban Pollutant Conversion Department of Environmental Science and Engineering University of Science and Technology of China

Hefei 230026, China

Key Laboratory of Advanced Marine Materials Ningbo Institute of Materials Technology and Engineering Chinese Academy of Sciences

Ningbo 315201, China

The ORCID identification number(s) for the author(s) of this article can be found under https://doi.org/10.1002/adfm.202423568

DOI: 10.1002/adfm.202423568

1. Introduction

Owing to the urgent need for environmental protection, energy conservation, and carbon dioxide (CO2) fixation to mitigate climate change and environmental energy crises, studies have recently focused on the electrochemical synthesis of urea.[1-5] Urea is one of the most commonly used nitrogen fertilizers and can be synthesized by a continuous reaction of $N_2 + H_2 \rightarrow NH_3$ and $NH_3 + CO_2 \rightarrow urea$, both of which are energy-intensive and demanding.[6,7] Urea production powered by renewable electricity using nitrate (NO3-) and CO2 as feedstocks is a promising alternative to the traditional method. However, the research demonstrating practical solutions for largescale urea electrosynthesis is limited.[8] The challenge is that the hydrogenation

processes for NO₃⁻ and CO₂ compete with each other. Furthermore, both processes should occur in nearly the same location for smooth C-N coupling. [9-12] With a few exceptions, side reactions, rather than urea production, dominate on multiple electrocatalysts owing to the overreduction of one reactant.[13,14] Thus, it is extremely important to develop an efficient electrocatalyst that can improve the C-N coupling efficiency of reduction reactions and inhibit harmful hydrogen evolution reactions (HER).

To date, numerous metal-based electrocatalysts have been investigated for C-N coupling to synthesize urea from CO₂ and NO3-, including noble metal- and non-noble metal-based catalysts.[15-20] However, the high price of precious metals and rare reserves in the earth's crust limit the large-scale commercial application of rare metal-based catalysts.[21] Among many non-precious metal catalysts, iron and iron carbon-based catalysts have attracted considerable attention because of their simple preparation, environmental protection, low cost, electrochemical activity, durability, and large-scale industrial application.[22-24] Owing to the isolated Fe-N active site, Fe-N-C exhibits high activity and selectivity for the electrocatalytic reduction of NO₃ or CO₂.[25] However, questions regarding the role of Fe-N-C coordination in determining the activity and product selectivity of such reactions remain. For example, the Fe-N-C site is relatively single, and the selectivity is insufficient in complex multisystems (such as NO₃⁻ and CO₂ co-reduction). [26,27] This easily leads to the dominant role of the side reaction of the NO₃ - electrocatalytic reduction to NH₃ (NITRR).^[28] To improve the efficiency

1616328,2.20.2,8, Downloaded from https://abranced.onlinebtary.wiley.com/doi/10.1002/adfm.202425386 by Aying wang - Ningbo Institute Of Materials, Wiley Online Library on (199/102025). See the Terms and Conditions (https://onlinebtary.wiley.com/ema-and-conditions) on Wiley Online Library for rules of use; OA actiles are governed by the applicable Creative Commons License

www.afm-journal.de

and selectivity of urea electrocatalytic synthesis, it is important to construct a multi-coupling catalytic center. Cerium oxide (CeO₂) is an inexpensive reducible metal oxide and an excellent carrier for metal catalysts in many catalytic processes, [29,30] such as CO₂ hydrogenation reactions. [31] As a catalyst carrier, CeO2 can uniformly disperse metals at various scales from the nanoscale to single atoms.[32] Among them, Ag monatomically anchored CeO₂ (Ag₁/CeO₂) demonstrated an excellent performance owing to the presence of oxygen vacancies (OVs). This led to the formation of an Ag-O-Ce3+ atomic interface, promoting CO2 adsorption and activation and reducing the *COOH-to-*CO reaction potential barrier.[33] Although the co-reduction reaction of NO₃- and CO₂ can improve the reduction ability of NO₃ and CO₂, the complex multi-proton- and multi-electron-transfer reaction pathway still hinders urea formation. [34,35] The co-reduction reaction involves the tandem generation and consumption of active hydrogen (H_{ads}) from water splitting in an aqueous medium.^[36,37] Considering that the high solubility of NO₃ and CO₂ is not fully harnessed, the excessive inhibition of water splitting (or compromise to competitive HER) results in an inadequate supply of H_{ads} for co-reduction reactions.[38-40] Thus, for urea electrosynthesis, rational strategies are urgently required to regulate the NITRR, electrochemical CO2 reduction (CO2RR), and HER processes to improve the key reaction kinetics.

In the complex process of urea electrosynthesis, reasonable strategies are required to scientifically regulate the NITRR, CO₂RR, and HER processes to improve the electrochemical synthesis rate and Faraday efficiency (FE). However, according to the existing literature, no research exists on this aspect presently, and the reaction mechanism remains unclear. Here, we selected a metal iron and cerium-based center, which is cheap, environmentally friendly, and has engineering application potential, to design a highly dispersed FeNC (FeNC-Ce) catalyst with OV-rich CeO₂ for urea electrosynthesis. In situ characterization and density functional calculation (DFT) were employed to reveal the mechanism and catalytic role of FeNC-Ce in urea electrosynthesis. The electrochemical properties of the FeNC and FeNC-Ce catalysts in single NITRR, CO₂RR, HER, and coupling systems were verified. The study showed that although FeNC performed well during a NITRR and was active against the CO2RR and HER, the intense competition among the three reduction processes led to low urea yields throughout the reaction pathway. Contrarily, FeNC-Ce triggered the moderate reduction of NO₃⁻, CO₂, and H₂O and enabled simple C-N coupling, providing extraordinary catalytic properties for urea electrosynthesis.

2. Results and Discussion

2.1. Synthesis and Structural Characterization of Electrocatalysts

FeNC was prepared via a two-step method using 2-aminoterephthalic acid and ferric chloride as nitrogen, carbon, and iron sources, respectively, whereas FeNC-M was obtained by the further addition of CeO₂ (Figure 1a). Scanning electron microscopy (SEM) showed that FeNC-Ce evolved from a triangular pyramid to an orderly hook shape (Figure 1b–f). The corresponding energy-dispersive X-ray spectroscopy (EDS) mapping of FeNC-Ce indicated the distribution of Fe/N/O/C/Ce atoms. The proportion of FeNC-Ce was as high as 84.04%,

and the high metal content was conducive to the exposure of metal active centers during the reaction (Table \$1, Supporting Information). Figure 1g shows low-magnification transmission electron microscopy (TEM) images of the sample, revealing hook structures. A HRTEM image (Figure 1h) revealed the interplanar spacings of 0.310 and 0.190 nm, assignable to the (1 1 1) and (2 0 0) planes of CeO₂ and Fe_{4.4}N, respectively.^[40,41] Figure 1i shows the X-ray powder diffraction (XRD) patterns of FeNC and FeNC-Ce. The diffraction peaks at the 2θ values of 44.992° and 64.816° were attributed to the (3 1 1) and (3 2 1) crystal planes of Fe₃C (PDF#35–0772), respectively.^[42] For the prepared FeNC-Ce, the peaks of 28.549°, 33.083°, 47.834°, and 69.581° corresponded to the (1 1 1), (2 0 0), and (2 0 0) crystal planes of CeO_2 (PDF#75-0151), [43] as well as $Fe_{44}N$ (PDF#03-0955), [40] respectively. XRD analysis suggested that NM8B tended to convert to Fe₃C and NM8B@CeO₂ tends to convert to FeNC at elevated temperatures. As shown in Figure 1j, the surface of the metallic oxide particles was negatively charged, promoting the adsorption of positively charged organic ligands onto the metallic oxide surface. This resulted in the acquisition of positive charges by FeNC-Ce (1.59 \pm 0.43 mV) and FeNC (1.9 \pm 0.33 mV), which enhanced the adsorption of NO₃⁻.

X-ray photoelectron spectroscopy (XPS) was conducted to ascertain the chemical functionalization and surface composition of FeNC and FeNC-Ce. In the O 1s spectra of FeNC and FeNC-Ce (Figure 2a), characteristic peaks at 529.2 \pm 0.2, 531.0 ± 0.2 , and 533.2 ± 0.2 eV corresponded to lattice O, C=O, and O=C-O,[44] respectively. In the C 1s spectra of FeNC, and FeNC-Ce (Figure 2b), characteristic peaks at 284.6 \pm 0.1, 285.7 \pm 0.2, and 288.8 \pm 0.2 eV corresponded to C=C/C-C,^[45] C-N, and O-C=O^[46] groups, respectively. The N 1s spectrum (Figure 2c) could be deconvoluted to identify pyridine N (≈398 eV),[47] graphitic N (≈400.5 eV), and oxidized N (\approx 402.6 eV) contributions. [48] The Fe 2p_{3/2} signals (Figure 2d) exhibited one peak assignable to Fe²⁺ (710.0 \pm 0.2 eV). [49] The Ce 3d signals (Figure 2e) exhibited peaks assignable to Ce³⁺ (885.2 eV), (898.9 eV) and (904.5 eV) and Ce4+ (882.00 eV), (897.9 eV), and (916.2 eV).[50] Vacancy defects in the sample were further identified via Electron paramagnetic resonance (EPR) spectroscopy (Figure 2f). FeNC-Ce exhibited higher signal peak intensity at g = 2.003 than FeNC, suggesting more OVs in the CeO₂-modified metal-organic framework (MOF) derivatives, which was consistent with the results of the Raman characterization.^[51] In Raman spectroscopy (Figure S1a, Supporting Information), the I_D/I_G ratio is an index to characterize the degree of graphitization of carbon components, [52] and the I_D/I_C ratio of FeNC-Ce (3.17 \pm 0.26) is higher than that of FeNC (1.78 \pm 0.16). This suggested that FeNC-Ce exhibited increased porosity and a large number of defective structures.

Figure S1b (Supporting Information) illustrates the magnetic curves of FeNC and FeNC-Ce. The metal oxide regulated the MIL-88B(Fe)-derived structure; it had been endowed with magnetic properties. Owing to the magnetic properties of the FeNC-Ce, the FeNC-Ce can be easily separated from the electrolyte. In addition, the FeNC-Ce composite maintained its magnetic properties after use, confirming its stable structure. Fourier-transform infrared spectroscopy (FT-IR) revealed two peaks at 1641 and 3456 cm $^{-1}$ in all the samples, attributed to the stretching vibrations of the C=C/C=N $^{[53]}$ and OH bonds, respectively (Figure S1c,

161 63028, 2025, 28, Downloadec

on linelibrary.wiley.com/doi/10.1002/adfm.202423568 by Alying wang - Ningbo Institute Of Materials , Wiley Online Library on [09/10/2025]. See the Terms

conditions) on Wiley Online Library for rules of use; OA articles are governed by the applicable Creative Commons

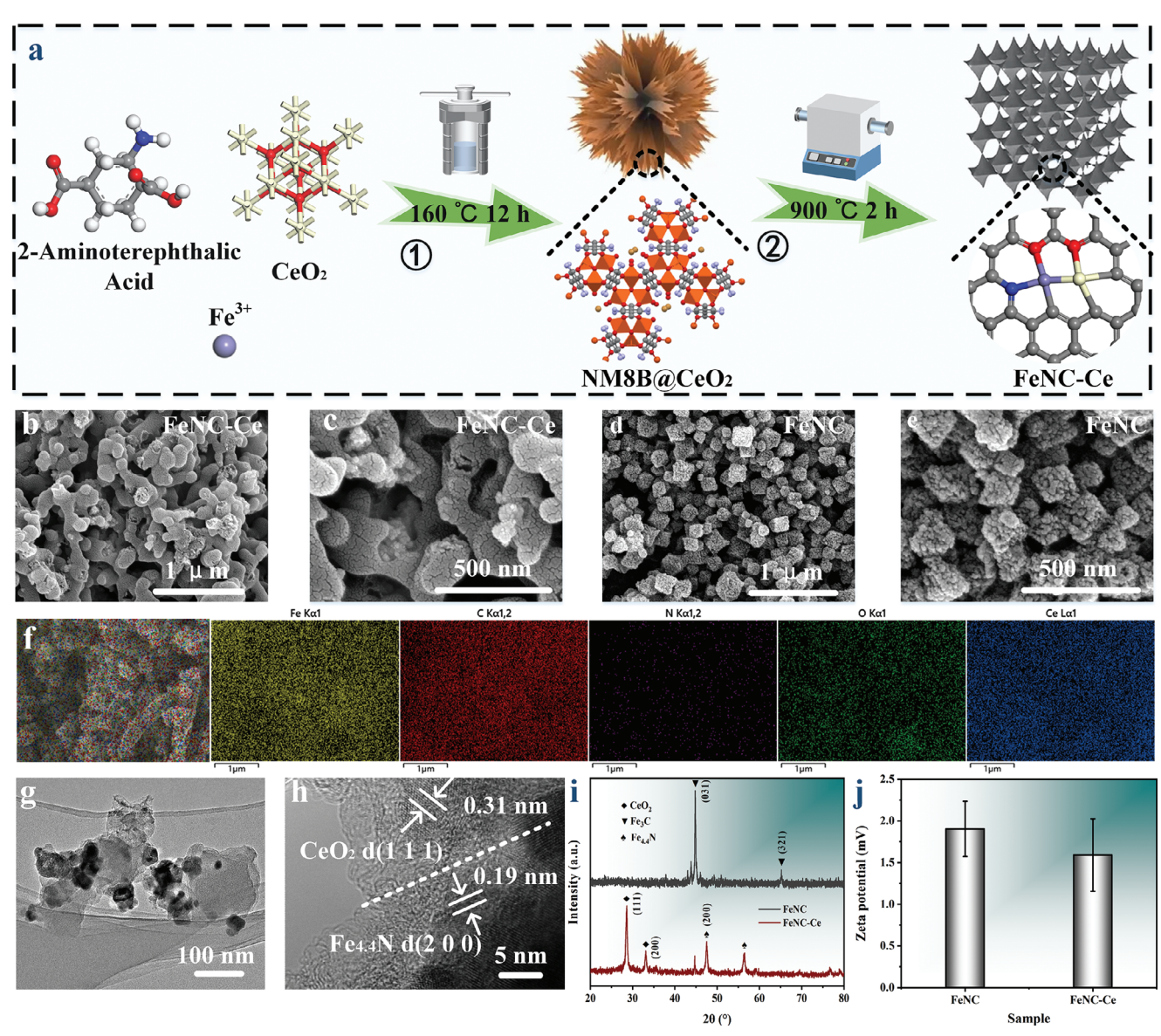


Figure 1. a) Schematic of the synthetic process. SEM images of b,c) FeNC-Ce and d,e) FeNC. f) EDS mapping of FeNC-Ce composition. g) TEM images. h) HRTEM images of FeNC-Ce. i), XRD patterns. j), Zeta potential.

Supporting Information). At different hydrothermal durations, no changes in surface groups were observed in FT-IR spectra. The CeO_2 modifications preserved some -C(=O)O- bonds, whereas the M-O bond remained largely untouched. [55]

2.2. Evaluation of Catalytic Performance

The electrocatalytic selectivity of FeNC-M and FeNC for urea synthesis was evaluated by chronoamperometry. FeNC exhibited an FE of below 40% toward urea with the overproducing by-products (Figure 3a), among which NITRR products (NO₂⁻ and NH₃) dominated in the entire potential range investigated. Unexpectedly, cerium-modified catalyst (FeNC-Ce) urea was the predominant reaction product (Figure 3b and Figure S4, Supporting Information). The FeNC-Ce catalyst enabled urea electrosynthesis

at a yield rate of 2690 \pm 88.3 µg mg⁻¹ h⁻¹ with a promising FE of 64.6% at −0.5 versus RHE (Figure 3c and Figure S5, Supporting Information). The maximum urea yield of FeNC-Ce was ≈ 3.79 times that of FeNC, and the effect significantly improved. Furthermore, the N-selectivity was determined based on the molar yield of N-containing products, indicating a high proportion of NO₃⁻ conversion to NO₂⁻. However, the FE of the NO₂⁻ product was rather limited, compared with that of urea, considering the extremely smaller number of transferred electrons for conversion into NO2- than urea. In addition, the yields of the by-products (H2 and CO) were low (Figure S6, Supporting Information). This property is one of the most critical characteristics of FeNC-Ce for its excellent urea selectivity. Considering that the synthesis process of FeNC and FeNC-Ce is almost the same, the main difference between them may stem from whether FeNC and O-Ce are added with or without Ce ions. Therefore,

onlinelibrary.wiley.com/doi/10.1002/adfm.202423568 by Alying wang - Ningbo Institute Of Materials

, Wiley Online Library on [09/10/2025]. See the Terms and Conditions (https://onlinelibrary.wiley

com/terms-and-conditions) on Wiley Online Library for rules of use; OA articles are governed by the applicable Creative Commons

www.afm-journal.de

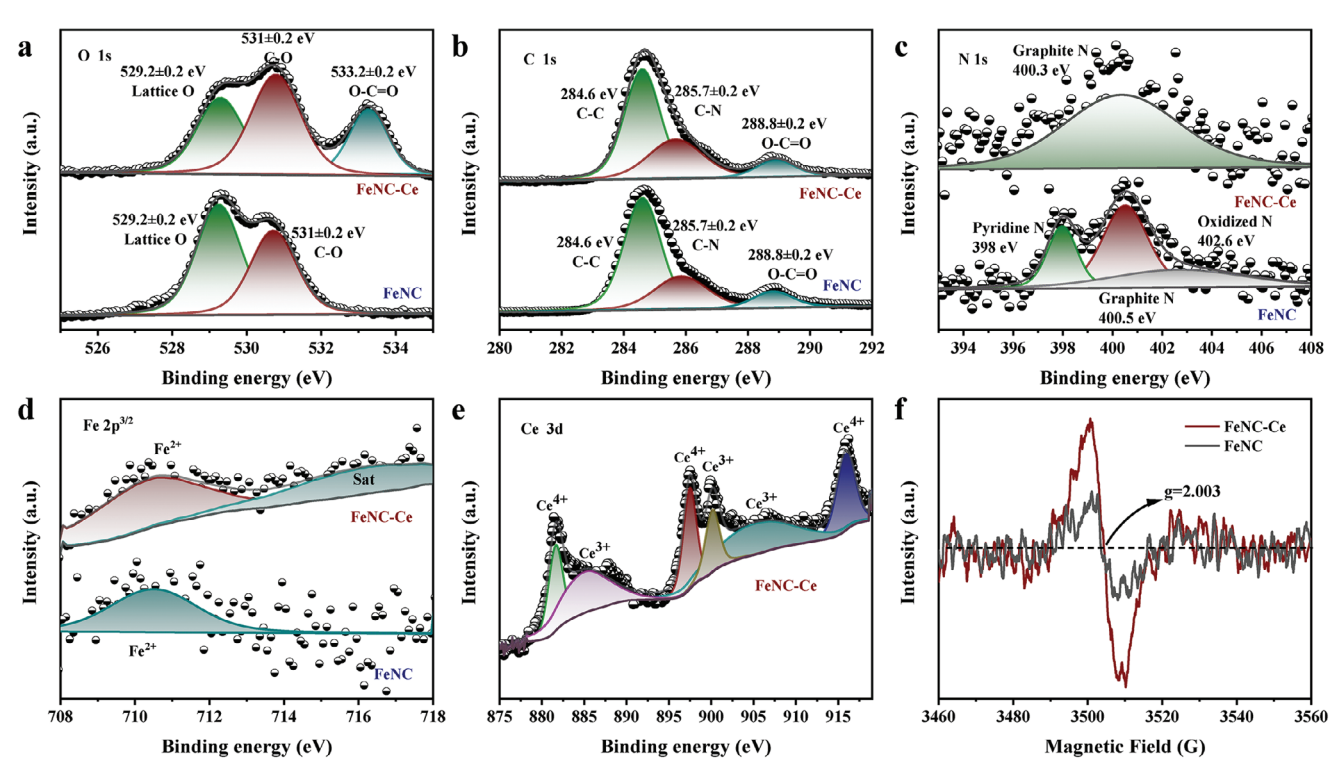


Figure 2. XPS spectra of a) O 1s, b) C 1s, c) N 1s d) Fe 2p, e) Ce 3d, and f) EPR spectra.

we assume that the huge difference in the performances of the urea synthesis was attributable to the two substances mentioned above, both of which can act as catalytic centers for the reduction of NO_3^- and CO_2 .

To evaluate the urea synthesis efficiency of FeNC-Ce, we performed electrocatalytic measurements in electrolytes with different NO₃ - concentrations (0.01, 0.1, and 1 м) (Figure S7, Supporting Information). The maximum urea electrosynthesis rate of the FeNC-Ce catalyst at 1 м KNO₃ + 0.1 м KHCO₃ and potential of -0.5 versus RHE reached 20 $969.2~\mu g~mg^{-1}~h^{-1}$ and FE_{max} of 89.3% (Figure S8, Supporting Information). The FeNC-Ce electrode exhibited considerable potential for the conversion of NO₃⁻/CO₂ into urea, with the associated FEs exceeding 40% under these conditions, reflecting the excellent sensitivity of the prepared electrode. The results showed that the yield of urea quantified by NMR method was equivalent to that obtained by the urease decomposition method (Figure S2, Supporting Information), which confirmed the reliability of this study in product quantitative analysis. These values were superior to those of recently reported catalysts (maximum urea yield of 200-2300 µg mg h^{-1} , FE_{max} of 11.5%–83.4%) working at similar potentials^[28,56–63] (Figure 3d). The durability test of FeNC-Ce revealed practically no degradation in either activity or urea selectivity for 16 successive runs for a total of 8 h (Figure 3e). After the 16 successive runs, SEM was performed (Figure 3f), and the results showed that the morphology of FeNC-Ce catalyst remained basically intact. The sustained electrocatalytic activity demonstrated the long-term stability of FeNC-Ce. This stability not only highlights its potential for practical applications but also provides support for further optimization of catalyst design. After 16 cycles of testing, the corresponding XPS results were analyzed (Figure S9a-e, Supporting Information). The species of C, Fe, and Ce changed little before and after the catalyst reaction, while the O and N signals of the non-metals showed slight variations. After the reaction, the lattice oxygen undergoes transformation and the non-metallic nitrogen changes from graphite nitrogen to pyridine nitrogen. In addition, it can be seen from the FT-IR analysis before and after the reaction that the main bond structure of the catalyst is still maintained (Figure S9f, Supporting Information). This result further proves the stability of the catalyst.

We examined other metal oxide support catalysts, including FeNC-Ti, FeNC-W, and FeNC-Zn, to co-reduce NO₃- and CO₂ (Figures \$10 and \$11, Supporting Information). Owing to the competitive NITRR, the urea production of the three catalysts was negligible. The seesaw between NO₃⁻ and CO₂ reduction was always tilted to the former, thereby hindering C-N coupling, which seems to be a common situation in carbon-supported metal catalysts. Figure S12 (Supporting Information) shows the effect of applied potentials on the yield rate of urea. Compared with FeNC-Ti, FeNC-Zn, and FeNC-W, the FeNC-Ce catalyst produced considerably higher yields within the range of -0.4 to -0.9 V versus RHE. Despite a larger total current density delivered by FeNC-Ti, FeNC-Zn, and FeNC-W, FeNC-Ce consumed most electrons to generate by-products, resulting in remarkably poor selectivity toward C-N coupling. Electrochemical impedance spectroscopy (EIS) tests revealed that the FeNC-Ce exhibited low charge-transfer resistance and excellent ion-transfer capacity (Figure \$13 and Table \$2, Supporting Information), probably due to the abundant porosity of the MOF-derived porous carbon, which enhanced ion transport, resulting in sufficient electron contact. The introduction of CeO₂ species increased resistance slightly, with the R_{ct} varying between 0.329 and 5.751 Ω , and the effect on overall resistance was

16163028, 2025, 28, Downloaded from https://advanced.onlinelibrary.wiley.com/doi/10.1002/adfm.202423568 by Aiying wang - Ningbo Institute Of Materials

, Wiley Online Library on [09/10/2025]. See the Terms and Conditions (https://onlinelibrary.wiley

s-and-conditions) on Wiley Online Library for rules of use; OA articles are governed by the applicable Creative Commons

www.afm-journal.de

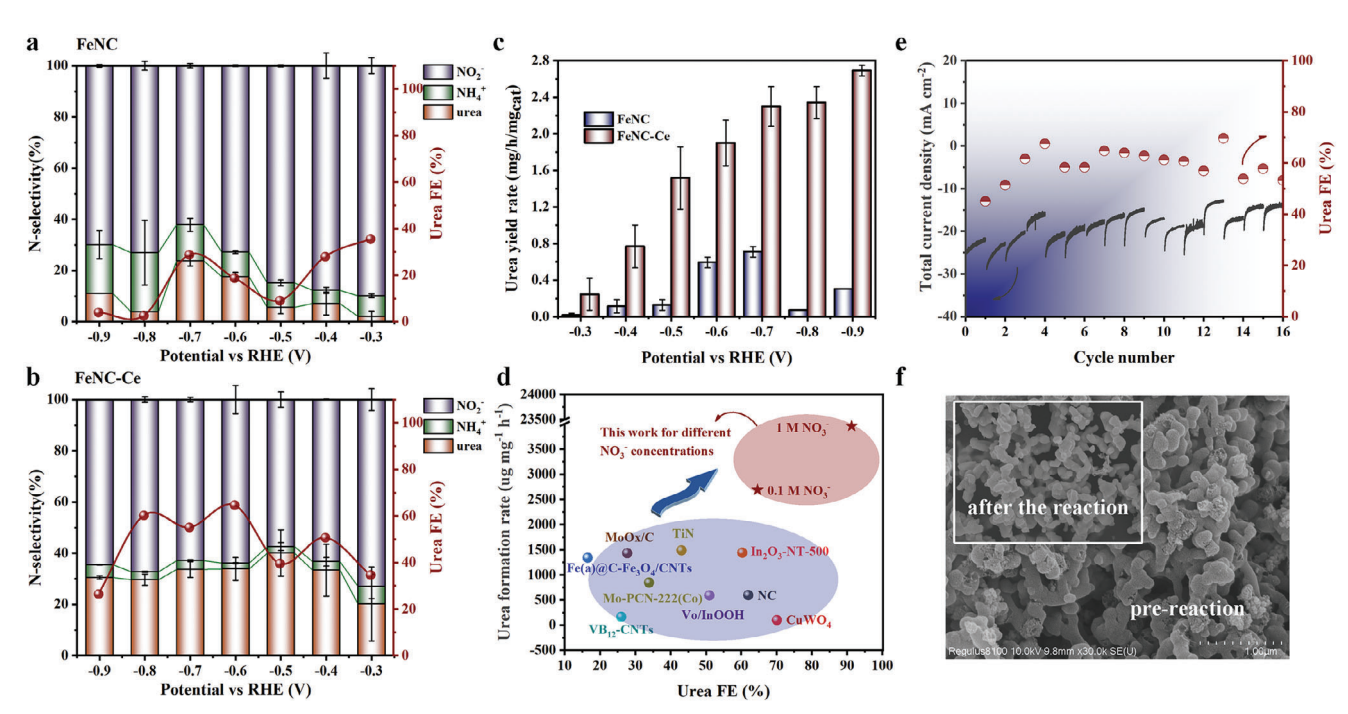


Figure 3. FEs of urea and N-selectivity of N-containing products on a) FeNC and b) FeNC-Ce. c) Urea yield rates. d) Comparison of urea formation rate and FE between FeNC-Ce and reported catalysts. e) Stability test of FeNC-Ce. f) SEM images of before and after the stability test.

negligible. The charging current was plotted at different scan rates (Figure S14a–e, Supporting Information) to obtain the double-layer capacitance ($C_{\rm dl}$) from the slope. Figure S14f (Supporting Information) shows a difference in the orders of magnitude in the $C_{\rm dl}$ between the films depending on the composition. Compared with the contrast electrode, the large specific capacitance of FeNC-Ce was 29.3 mF cm⁻², indicating that FeNC-Ce has great potential in electrochemical applications.

2.3. Origin of C-N Bond Formation and Reaction Mechanism

2.3.1. Tracking of Electrochemical Processes and Evolution of Catalyst

Operando ATR-SEIRAS can provide a better understanding of the NO₃⁻ and CO₂ co-reduction mechanism on the FeNC-Ce catalyst. Three bands around 893, 1127, 1600–1700, and 900–1000 cm⁻¹ were assignable to C—O, C=O, and N—H, respectively, ^[64,65] both of which exhibited a marked increase in intensity from –0.3 to –0.9 V (**Figures 4**a–b and \$15, Supporting Information). In the same system, there may have been a certain mismatch between the rates of the NITRR and CO₂RR. This was because the strength of the N—H bond exceeded that of the C—O bond during the co-reduction process. The bands centered around 1228 cm⁻¹ corresponded to the C—N stretching vibration of the reaction intermediates. ^[28] In the voltage range of –0.3 to –0.9 V, their intensity increased steadily and modestly evolved afterward, reflecting the successful coupling of C—N and the production of urea during the co-reduction of NO₃⁻ and CO₂.

ATR-SEIRAS revealed that the CO_2RR process may be slower than the NITRR process. In addition, FeNC-Ce had better urea

synthesis yield and selectivity than FeNC, which may be related to the CO₂RR process. To further verify the aforementioned speculation, CO2-TPD and CO-TPD were conducted to evaluate the thermodynamic adsorption energy of *CO₂ and the intermediate *CO on the surface of FeNC and FeNC-Ce. For the CO₂-TPD measurements (Figure 4c), the peak strength of CO2 desorption for FeNC-Ce in high-temperature regions exceeded that in the case of FeNC, indicating that FeNC-Ce exhibited a stronger chemical adsorption capacity. Thus, compared with FeNC, FeNC-Ce exhibited better adsorption and stabilization capacity for *CO₂ and *CO intermediates, which may have helped to accelerate the CO2RR process. As shown in Figure 4d, FeNC and FeNC-Ce exhibited good adsorption capacity for CO with a desorption peak in the low-temperature region (<200 °C) and multiple desorption peaks in the high-temperature region (200-400 °C). This represented the chemical and physical adsorptions of CO on the surface, respectively. Under the influence of CeO2, the physical and chemical adsorption of CO by FeNC-Ce significantly increased, along with the favorable adsorption capability of Ce sites for the *CO intermediate.

The HER process is one of the key steps in urea production. Hydrogen content from FeNC-Ce was significantly lower than that from FeNC, indicating that the hydrogen protons in FeNC-Ce primarily facilitated the production of urea or intermediates rather than yielding hydrogen by-products (Figure S6, Supporting Information). Thus, we believe that the NITRR is stronger than the $\rm CO_2RR$ during co-reduction. FeNC-Ce exhibited a better performance of urea production because the introduction of Ce species enhanced the $\rm CO_2RR$ and reduced the production of the by-product ($\rm H_2$), thereby improving the activity and selectivity of urea electrosynthesis.

onlinelbrary.wiley.com/doi/10.1002/adfm.202423568 by Aying wang - Ningob Institute Of Materia k. Wiley Online Library on (19/102025). See the Terms and Conditions (https://onlinelibrary.wiley.com/terms-and-conditions) on Wiley Online Library for rules of use; OA articles are governed by the applicable Cerative Commons.

www.afm-journal.de

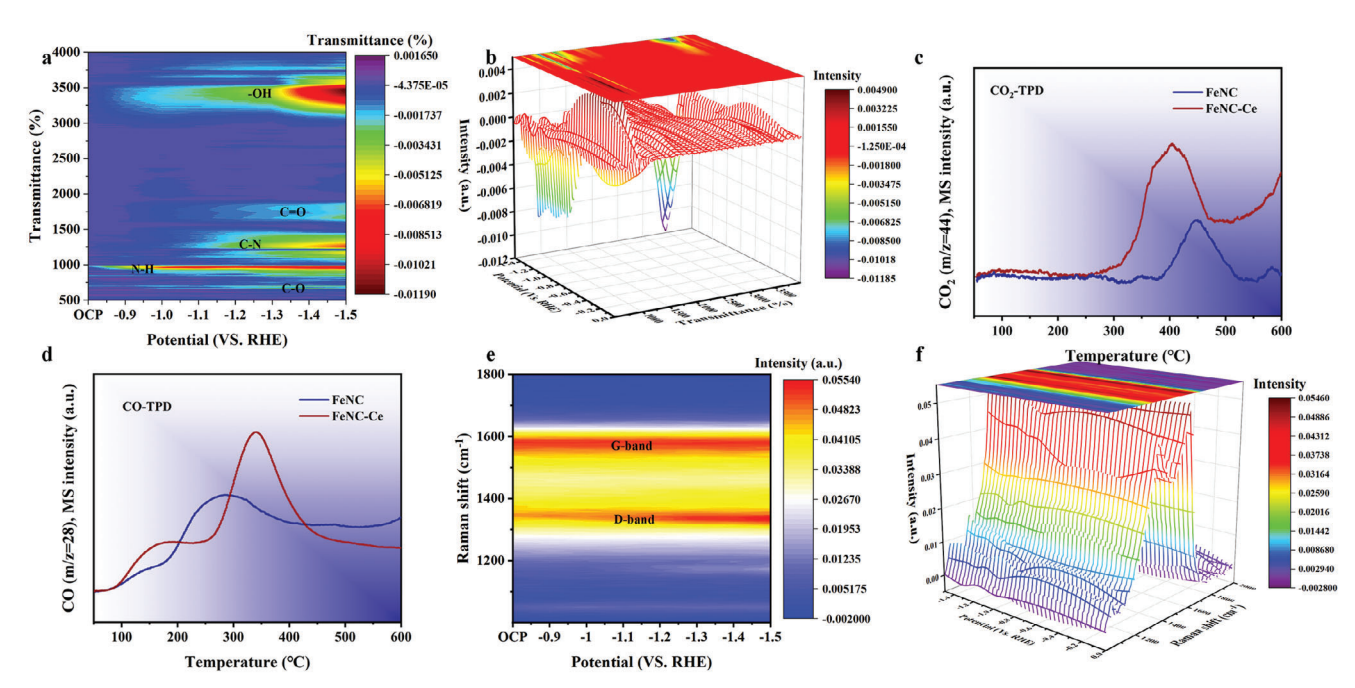


Figure 4. a) ATR-SEIRAS and b) 3D ATR-SEIRAS spectra of FeNC-Ce at different applied potentials during the co-reduction of CO_2 and NO_3^- . c) CO_2 -temperature program desorption (TPD). d) CO-TPD. e) In situ and f) 3D Raman spectra of FeNC-Ce at different applied potentials during the co-reduction of CO_2 and NO_3^- .

To determine the role of each catalyst component in the electrochemical synthesis of urea, in situ Raman spectroscopy was used to monitor the FeNC-Ce during the catalytic reaction. A peak at 1050 cm⁻¹ corresponding to the symmetrical stretching mode of NO₃⁻ was observed (Figure 4e–f and Figure S16, Supporting Information). [66,67] The peaks observed at 1170 and 1417 cm⁻¹ were assignable to the stretching vibrations of —NH₂ and C—N, [68,69] respectively, which increased with an increase in potential, indicating their formation in the co-reduction of NO₃⁻ and CO₂. Furthermore, we observed that the intensity of the D-band corresponding to 1580 cm⁻¹ increased as the co-reduction progressed, indicating that the defective carbon played a crucial role in the co-reduction stage.

2.3.2. Mechanism of C—N Coupling via Cooperative Electroreduction Through NITRR, CO_2RR , and HER

To better understand the electrocatalytic property of FeNC-Ce, we conducted different experiments to evaluate its activity during the NITRR, CO₂RR, and HER, separately. In the individual NITRR, argon gas was fed into the electrolyte, instead of CO₂. FeNC delivered a considerably higher NITRR current density than FeNC-Ce (**Figure 5a**). This suggests that the simple NM8B-derived system (FeNC) promoted the maximum reduction of NO₃⁻ compared with the modified system (FeNC-Ce). However, as shown in the figure below, the urea selectivity would be adversely affected by the simple NITRR process when the CO₂RR process demonstrates considerably inferior activity during the NITRR. Although the derived CO₂RR current densities were similar for FeNC-Ce and FeNC, they were one order of magnitude smaller than the NITRR current densities in individual NO₃⁻ reductions

(Figure 5b and Figure S17, Supporting Information). For another side reaction of the HER process, a simple HER process may adversely affect the urea selectivity or current utilization efficiency if the cathode current is mainly contributed to the HER. [70,71] We observed that FeNC can deliver a significantly higher HER current density than FeNC-Ce (Figure 5c). With the balance between the NITRR, HER, and $\rm CO_2RR$ achieved during the co-reduction of $\rm NO_3^-$ and $\rm CO_2$, there would be limited opportunity for urea formation at a single catalytic center if the activity of this site remained unchanged during the reactions.

On FeNC-Ce, the CO₂ conversion rate obtained by the coreductive yield of urea and CO exceeds the conversion rate of individual CO₂RR (Figure 5d). This indicates that the presence of NO₃⁻ can activate the electrochemical conversion of CO₂. Based on previous studies, we ruled out the possibility of CO₂ coupling with C—N, the main intermediate of NITRR.^[28] Thus, urea formation requires CO2 hydrogenation, particularly the rate-determining *CO₂→*CO step in CO₂RR. In this case, facilitating CO₂ conversion implied that the NITRR process played an important role in reducing the energy consumption of this fundamental step. This reduction can be explained by NITRR-induced changes in catalytic activity. Over the FeNC-Ce catalyst, the conversion rate of NO₃ - significantly increased after the introduction of CO₂ as a reactant (Figure 5e). This implied that the NITRR intermediates could participate in urea formation but appeared capable of being activated from the CO₂RR intermediates.^[28] In this context, NO₃ was first reduced at the catalytic center, and the reaction proceeded to NO2- through two hydrogenation steps (change in valency of N from +5 to +3). Here, various NO₃-, NO₂-, and CO₂ coupling systems were designed, and NO₂-coupled CO₂ systems were observed to be more conducive to C-N coupling than NO₃⁻-coupled CO₂ systems (Figure S18, Supporting

16163028, 2025, 28. Downloaded from https://advanced.onlinelibrary.wiley.com/doi/10.1002/adfm.202423568 by Alying wang - Ningbo Institute Of Materials , Wiley Online Library on [09/10/2025]. See the Terms and Conditions (https://onlinelibrary.wiley

com/terms-and-conditions) on Wiley Online Library for rules of use; OA articles are governed by the applicable Creative Commons

www.afm-journal.de

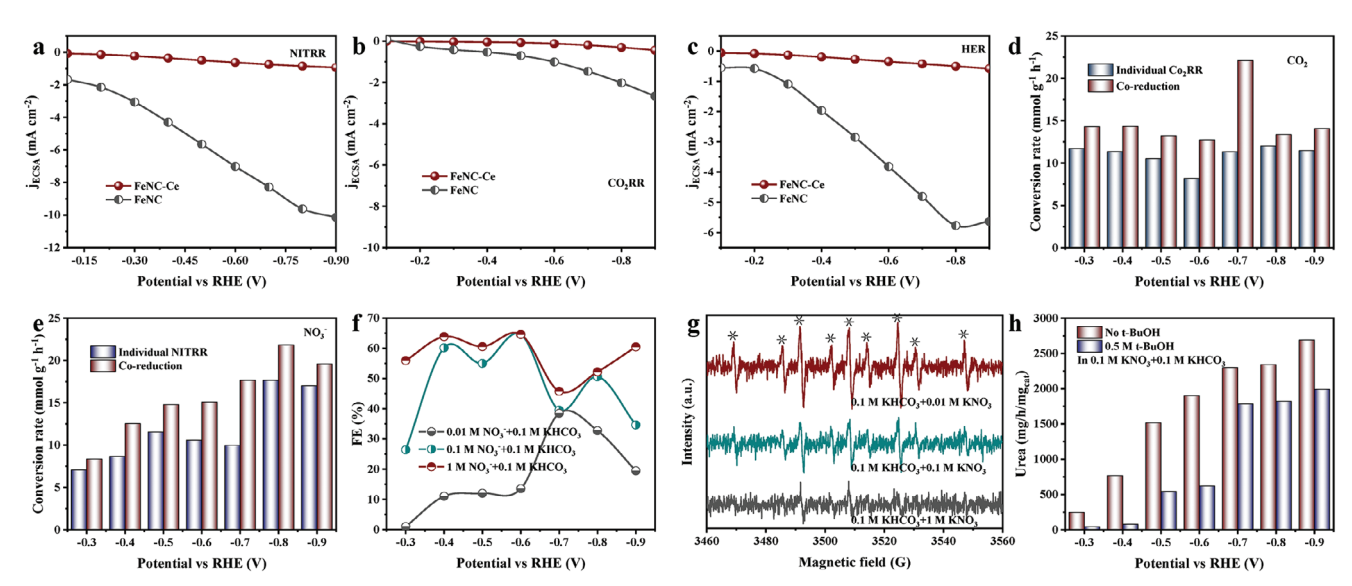


Figure 5. Control experiments of individual NITRR, HER, and CO_2RR . Current density during the individual reduction of a) NO_3^- , b) CO_2 , and c) H_2O . d) Rate of conversion of CO_2 into C-containing products on FeNC-Ce during individual CO_2RR compared with co-reduction reaction. e) Rate of conversion of NO_3^- into N-containing products on FeNC-Ce in individual NITRR compared with co-reduction reaction. f) urea FEs and g) EPR spectra of solutions catalyzed by FeNC-Ce with different COO_3^- . h) Urea yield rates over FeNC-Ce with and without 0.5 M tertiary butanol (t-BuOH) as a quencher.

Information). When NO₂⁻-coupled CO₂ systems were injected at different concentration gradients, C—N coupling became more intense with an increase in the concentration of NO₂⁻, suggesting that the switch of the reaction path to CO₂RR was probably accomplished in the period of N intermediate formation. Subsequently, CO₂RR occurred in the vicinity of the formed NITRR products, and the CO₂RR intermediates readily combined with the N intermediate to produce urea.

Owing to the remarkable performance of FeNC-Ce under various electrolyte conditions, we conducted experiments to describe the relationship between the urea production and H_{ads}. Considering that the N-containing intermediates that react with H_{ads} were derived from initial NO₃⁻, the concentration of NO₃⁻ (cNO₃⁻) significantly affected the consumption capacity of H_{ads}. We assessed the urea efficiency of FeNC-Ce at different cNO_3^- in 0.1 M KHCO₃ (Figure S7, Supporting Information). In the low potential range (-0.3 V vs RHE), cNO₃ had no significant effect on urea production due to the limited rate of H_{ads} production, which constrained NO₃⁻ conversion (Figure 5f). However, the urea yield increased with an increase in FE as cNO₃⁻ increased at more negative potentials, suggesting that an adequate supply of H_{ads} under these conditions sustained the Hads homeostasia and inhibited competing HER, thereby optimizing the urea production.[72] To substantiate the rapid conversion of Hads, cNH3 was quantified via uv-vis spectroscopy under various test configurations. The findings revealed that C_{NH3} on FeNC-Ce was consistently lower than that of urea under the same potential with different electrolyte configurations, indicating that the utilization efficiency of $\mathbf{H}_{\mathrm{ads}}$ was very high (Figure S7, Supporting Information). A positive correlation between cNO_3^- and cNO_2^- suggested that an adequate supply of H_{ads} markedly enhanced the conversion of intermediates into urea. The EPR spectra of FeNC-Ce were recorded in 0.1 м КНСО₃ with varying NO₃⁻ concentrations (Figure 5g). The intensity of the 5,5-dimethyl-1-pyrroline N-oxide (DMPO) signals decreased with an increase in cNO₃⁻, vanishing entirely at 1.0 м

 ${\rm cNO_3}^-$. This demonstrated that ${\rm H_{ads}}$ produced by water splitting was consumed during the NITRR process, which was consistent with the results of the ${\rm H_{ads}}$ trapping experiment (Figure 5h), and highlights the critical role of ${\rm H_{ads}}$ balance in NITRR.

2.3.3. Theoretical Investigation of Catalysts and Cooperative Electroreduction Processes

To further determine the fundamental origin of the high selectivity of FeNC-Ce, DFT calculations on the FeNC-Ce crystal corresponding to the TEM and XRD results were conducted. The adsorption process is the premise and cornerstone of catalytic reactions, and understanding the adsorption process that plays an important role in all electrocatalytic reactions is essential for designing effective electrocatalysts. [73,74] Thus, we first investigated the adsorption behavior of CO₂ and NO₃ on the surface of the aforementioned model. For CO₂ adsorption, the negative adsorption free energy of FeNC-Ce was -0.99 eV (ΔG_{*CO2}), exceeding that of FeNC (-0.96 eV), which was consistent with the CO₂ thermodynamic results obtained after TPD (Table \$3, Supporting Information). The NO₃⁻ adsorption free energy (ΔG_{*NO3}) values for FeNC-Ce and FeNC were -1.99 and -2.26 eV, respectively (Table S4, Supporting Information). The introduction of Ce sites helped the catalyst to adsorb CO2 and reduce NO3- adsorption to an

Considering that urea electrosynthesis involves nitrate reduction and CO_2 reduction, understanding the intrinsic links among single-system NITRR, CO_2 RR, and HER processes and catalysts is critical for efficient urea systems. The generation of *NH $_3$ is an important step in urea production, reflecting the difficulty of NO_3^- reduction. **Figure 6a** shows the free energy profiles of the reduction of NO_3^- into *NH $_3$; the reduction steps of NO_3^- into *NH $_3$ in the two modes were not spontaneous processes. The main potential-determination step (PDS) on FeNC-Ce was the

.com/doi/10.1002/adfm.202423568 by Aiying wang - Ningbo Institute Of Materials

, Wiley Online Library on [09/10/2025]. See the Terms

conditions) on Wiley Online Library for rules of use; OA articles are governed by the applicable Creative Commons

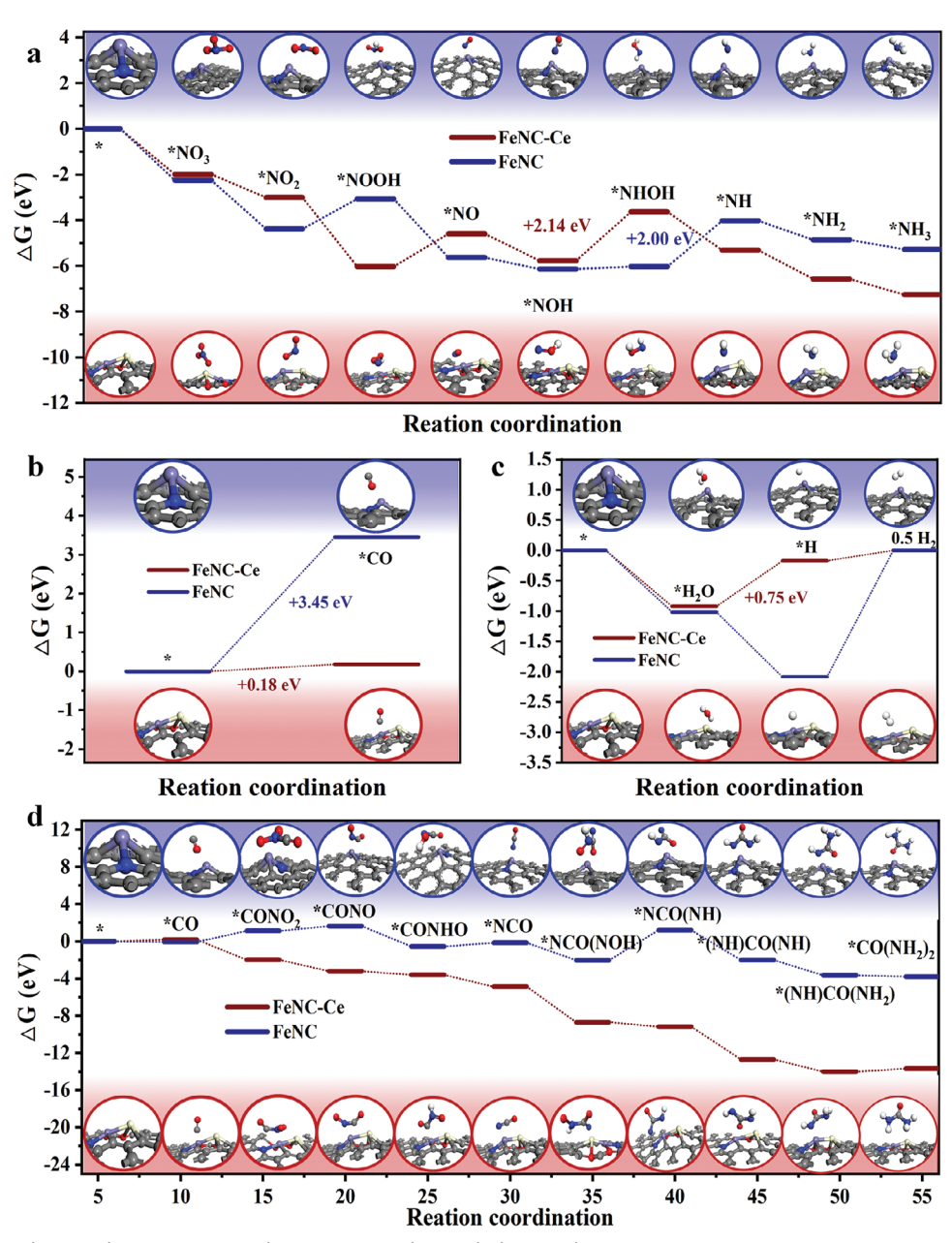


Figure 6. Free energy diagram during a a) NITRR, b) CO₂RR, c) and HER. d) the co-reduction reaction.

*NOH→*NHOH process with an energy barrier of 2.14 eV. For comparison, the PDS on FeNC was the *NHOH→*NH with a high energy barrier of 2.00 eV. The role of FeNC and Ce centers is shown in the multistage step map of NITRR, indicating that the free energy required for the introduction of Ce sites exceeded that of pure FeNC sites. Thus, FeNC sites are mainly responsible for the reaction with NO₃⁻ on FeNC-Ce. The experimental results showed that the reduction process of CO₂ was slower than that of NO₃⁻; however, the relationship between the key intermediates and catalyst has not been revealed. Thus, we established a relationship between the most important intermediate *CO for CO₂RR and the catalytic center. The *CO₂ electroreduction to *CO was endothermic by 0.028 and 3.45 eV for FeNC-Ce

and FeNC, respectively (Figure 6b). The direct conversion of *CO_2 into *CO on the FeNC-Ce surface was energetically more favorable than that on the FeNC surface. The innovative coupling of the Ce site and FeNC significantly improved the CO_2RR . As previously mentioned, the HER process is a key step in urea production. The experimental results showed that the right amount of H_{ads} can promote the co-reduction reaction; however, the relationship between the HER process and the NITRR, CO_2RR , and co-reduction processes was competitive. The DFT calculation results (Figure 6c and Table S5, Supporting Information) showed that the FeNC-Ce catalyst was inert toward the HER, a side reaction with a reaction-free energy of 0.75 eV, demonstrating the superior resistance of the HER. Conversely, the reaction free

6163028, 2025, 28, Downloaded from https://advanced.onlinelibrary.wiley.com/doi/10.1002/adfm.202423568 by Alying wang - Ningbo Institute Of Materials

, Wiley Online Library on [09/10/2025]. See the Terms and Conditions (https://onlinelibrary.wiley

and-conditions) on Wiley Online Library for rules of use; OA articles are governed by the applicable Creative Commons

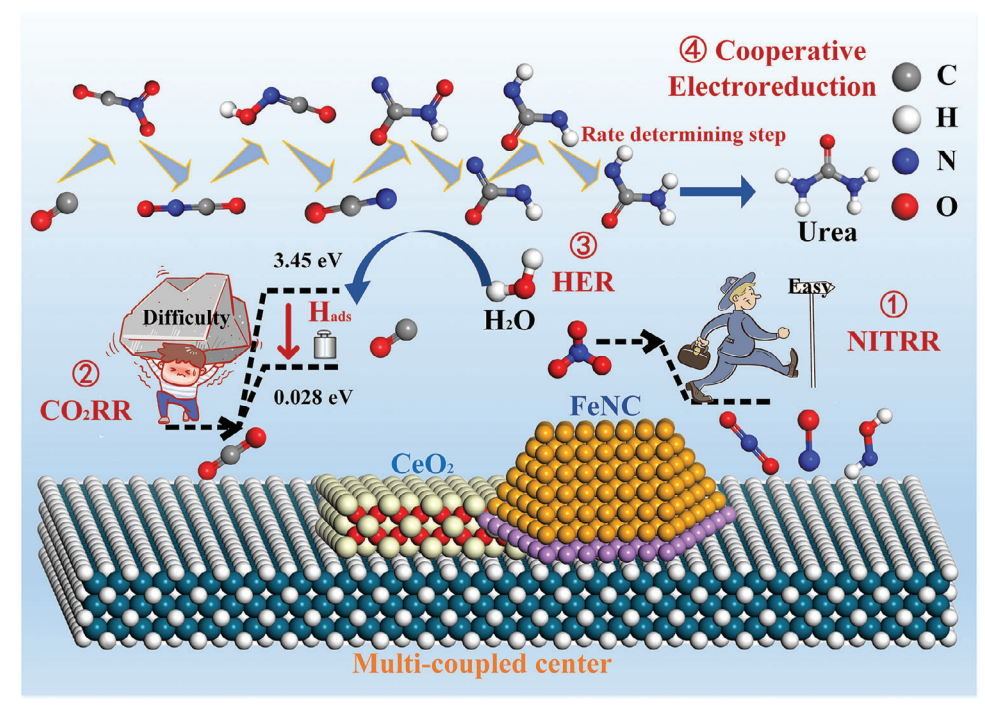


Figure 7. Mechanism of NO₃⁻ and CO₂ co-reduction reaction.

energy of HER on FeNC was -1.07 eV. This showed that between the electrosynthetic urea and HER, FeNC was more competitive than FeNC-Ce in the HER process. After theoretical studies on multiple side reactions, we observed that FeNC active species were frequently associated with a high NITRR and HER. Furthermore, coupling to promote $\mathrm{CO_2RR}$ active species (such as cerium species) reduced the overwhelming single-system reduction and minimized the formation of by-products.

For the co-reduction system, experiments showed that various nitrogen and carbon intermediates may have contributed to the urea synthesis. To clarify the possible synthesis path of this system, we simulated various N-containing intermediates and coupled reported C-N intermediates and catalysts^[75-77] to determine the relationship between the rate-limiting steps in urea synthesis and the catalytic active center. Figure 6d and Table S6 (Supporting Information) show the free energies of the intermediates in each step of the urea synthesis. The FeNC decisive steps included the formation process of *CONO₂ → *CONO, *CONHO \rightarrow *NCO, *NCO(NOH) \rightarrow *NCO(NH), with free energies of 1.19, 0.51, and 3.21 eV, respectively. Unexpectedly, for FeNC-Ce samples, the overall reaction pathway exhibited a kinetically feasible downward trend, indicating that FeNC-Ce had a naturally optimized catalytic site for electrocatalytic urea synthesis under environmental conditions. The introduction of the Ce species significantly promoted the co-reduction process and alleviated the one-sided NITRR process.

2.3.4. Catalytic Reaction Mechanism

Based on the above discussion, the electron transfer conversion mechanism within FeNC-Ce mainly encompasses three

stages: NITRR, CO2RR, HER, and cooperative electroreduction (Figure 7). In this system, the FeNC co-reduction process is mainly NITRR, whereas the CO₂RR process is relatively slow, indicating an overwhelming single-system reduction. The introduction of Ce species accelerated the adsorption of CO₂ and the intermediate CO and significantly decreased the energy barrier of * $CO_2 \rightarrow *CO$ (3.45 $\rightarrow 0.028$ eV). With the introduction of CeO₂ species, the HER changed from spontaneous to nonspontaneous ($-1.75 \rightarrow 0.75$ eV), which reduced the competitive reduction of the HER. Furthermore, the intermediate product (H_{ads}) can promote the hydrogenation process. Surprisingly, the overall reaction pathway showed a kinetically feasible downward trend, except that the $(NH)CO(NH_2) \rightarrow CO(NH_2)_2$ showed a certain rate-limiting step (0.34 eV), suggesting that FeNC-Ce has a naturally optimized catalytic site for electrocatalytic urea synthesis under environmental conditions. Thus, the system regulates the HER, NITRR, CO2RR, and coupling processes through dual active centers (FeNC and Ce-O), thereby mitigating overwhelming monoreduction and achieving high urea yield and FE.

3. Conclusion

This study proposed the competitive role of three reduction reactions (NITRR, CO_2RR , and HER) in the electrochemical synthesis of urea and achieved a balance among the three competitive reactions in the co-reduction system using the FeNC-Ce electrocatalyst as a paradigm. The FeNC-Ce had a maximum urea yield of 20 969.2 $\mu g \ mg^{-1} \ h^{-1}$ and FE_{max} of up to 89.3%, which were the highest values among all the reported values for urea production. This high yield suggested a high application potential for CO_2 capture, NO_3^- reduction, etc. Various characterizations and DFT calculations showed that the dominant reaction of the

www.afm-journal.de

FeNC cathode system was the NITRR reaction, and the CO₂RR process was the major rate-limiting step. When coupled with an OV-rich Ce metal center, the CO₂RR process was enhanced, and the moderate H_{ads} accelerated the co-reduction reaction, thereby increasing urea yield and current efficiency. This coupled system can confer a high propensity to urea production, resulting in an unprecedented inhibition of side reactions and providing a strategy for designing highly selective urea electrosynthesis catalysts.

4. Experimental Section

Syntheses of FeNC and FeNC-M: Syntheses of NM8B@MO: 2aminoterephthalic acid, FeCl₃ 6H₂O, as well as CeO₂, WO₃, ZnO, and TiO₂ were dispersed in N, N-dimethylformamide (30 mL) via ultrasonication at a molar ratio of 3:3:1. The obtained mixture was reacted in the oven at 160 °C for 12 h, and the product (NM8 B@MO) was washed three times with deionized water and ethanol, respectively. NM8B was synthesized in the same way as NM8 B@MO, except that MO was not added.

Syntheses of FeNC-M: NM8B or NM8 B@MO was heated under flowing N_2 at 900 °C for 2 h to form FeNC or FeNC-M.

Ex Situ and In Situ Characterizations: Ex situ characterizations: Further details on XRD, SEM, EDS, TEM, XPS, Raman spectroscopy, FT-IR, zeta potential, Inductively coupled plasma-optical emission spectroscopy (ICP-OES), EPR spectra, thermal conductivity detector (TCD), TPD, were available in the supporting information.

In Situ Characterizations: Electrochemical attenuated Total Reflection surface-enhanced infrared absorption Spectroscopy (ATR-SEIRAS) was performed using INVENIO R FTIR spectroscopy (Bruker). The reference electrode and the counter electrode were consistent with the electrochemical test. The co-reduction reaction of NO₃⁻ and CO₂ was carried out with CO_2 saturated electrolyte (0.1 M KNO3 and 0.1 M KHCO3). In situ Raman characterization was performed using the confocal microscope Raman System (Renishaw inVia) at a test wavelength of

Electrochemical Measurements: All the electrochemical measurements were conducted using a CHI 760E electrochemical station in a threeelectrode H-cell electrolyzer. The catalyst powders (0.01 g) and Nafion solution (100 uL) were dissolved in ethanol (900 uL) as the ink. Then, the catalyst ink was coated on 1×1 cm² copper foam, and the working electrode with a load capacity of 2 mg cm⁻² was obtained after drying. In addition, a platinum foil and an Ag/AgCl (saturated KCl) electrode were used as counter electrode and reference electrode, respectively, and the chamber was separated by Nafion 117 membrane (DuPont). For each experiment, the applied potential was converted using a reversible hydrogen electrode. Linear sweep voltammetry (LSV) curves and Cyclic voltammetry (CV) with/without NaNO3 in the circulating electrolyte were performed at a scan rate of 5 mV s⁻¹. Electrochemical double-layer capacity (EDLC) was determined via CV, which was recorded within a potential range of 0.1 V around open-circuit potential (OCP) to prevent apparent Faradaic processes. The response current values (I_a and I_c) and C_{dl} were determined from the CV test. The C_{dl} was calculated using the I_a and I_c and regarded as an indicator of the active site number.

$$\frac{\mathsf{Ia} - \mathsf{Ic}}{2} = C_{dl}\mathsf{v} \tag{1}$$

EIS measurements were conducted in an impressed potential window with -0.02 V. The urea FEs and yield were determined by potentiostatic test for 0.5 h at the stirring rate of 400 rpm under different potentials (from -0.5 to -0.9 V vs RHE).

Further details on the materials, determination of the concentration of N-containing species and gas, ex situ characterizations, and computational methods, are available in the Supporting Information.

Supporting Information

Supporting Information is available from the Wiley Online Library or from the author.

Acknowledgements

This work was supported by the Jiangxi Province "Double Thousand Plan" Innovation Leading Talent Long Term Project (S2021CQKJ0696), Key Projects of Jiangxi Natural Science Foundation (20232ACB203009), Key R&D projects in Jiangxi Province (20223BBF61019), the Ministry of Education's Industry University Cooperation Collaborative Education Project of China (230724572207282), National Natural Science Foundation of China (52070094), First class undergraduate course construction project and Student innovation and entrepreneurship training program of Nanchang University (202210403102 and S202210403083). The authors would like to thank Ye Lin from Shiyanjia Lab (www.shiyanjia.com) for the XPS.

Conflict of Interest

The authors declare no conflict of interest.

Author Contributions

Y.Z. did investigation, data curation, and wrote the original draft. J.H., H.Z., W.X. and H.D. did investigation. Y.Z. and Z.Y. did methodology. Q.W., L.C., Z.Y. and J.Y. did investigation, methodology. W.L. performed visualization, supervision, reviewed & Editing. J.X. and S.C. did conceptualization, methodology. A.W. performed software, Investigation. X.X. did review & Editing, funding acquisition, supervision.

Data Availability Statement

Research data are not shared.

Keywords

carbon capture, C-N coupling, electrocatalysis, nitrate recycling, urea synthesis

> Received: December 2, 2024 Revised: February 7, 2025 Published online: February 16, 2025

1616328.2.20.2.5. 20. Downloaded from https://dvanced.onlinelbrary.wile.go.om/doi/10.1002/adfm.202423588 by Aiying wang - Ningbo Institute Of Materiah & Wiley Online Library on (19/1/2002). See the Terms and Conditions (https://onlinelibrary.wiley.com/terms-and-conditions) on Wiley Online Library for rules of use; OA articles are governed by the applicable Centure Commons.

- [1] H. Li, L. Xu, S. Bo, Y. Wang, H. Xu, C. Chen, R. Miao, D. Chen, K. Zhang, Q. Liu, J. Shen, H. Shao, J. Jia, S. Wang, Nat. Commun. 2024, 15, 8858.
- [2] J. Mukherjee, S. Paul, A. Adalder, S. Kapse, R. Thapa, S. Mandal, B. Ghorai, S. Sarkar, U. K. Ghorai, Adv. Funct. Mater. 2022, 32, 2200882.
- [3] S. Paul, A. Adalder, U. K. Ghorai, Mater. Chem. Front. 2023, 7, 3820.
- [4] S. Paul, S. Sarkar, A. Adalder, A. Banerjee, U. K. Ghorai, J. Mater. Chem. A 2023, 11, 13249.
- [5] Waghela S. R., Adalder A., Mitra K., et al., ChemCatChem 202401565.
- [6] B. H. Ko, B. Hasa, H. Shin, Y. Zhao, F. Jiao, J. Am. Chem. Soc. 2022, 144, 1258,
- [7] H. Shen, C. Choi, J. Masa, X. Li, J. Qiu, Y. Jung, Z. Sun, Chem 2021, 7,
- [8] M. Shibata, K. Yoshida, N. Furuya, J. Electroanal. Chem. 1995, 387,

.com/doi/10.1002/adfm.202423568 by Aiying wang - Ningbo Institute Of Materials

, Wiley Online Library on [09/10/2025]. See the Terms and Conditions (https://onlinelibrary

and-conditions) on Wiley Online Library for rules of use; OA articles are governed by the applicable Creative Commons

- [9] X. Zhu, M. Ge, X. Yuan, Y. Wang, Y. Tang, Applied Catalysis B: Environment and Energy 2025, 363, 124826.
- [10] S. Shin, S. Sultan, Z.-X. Chen, H. Lee, H. Choi, T.-U. Wi, C. Park, T. Kim, C. Lee, J. Jeong, H. Shin, T.-H. Kim, H. Ju, H. C. Yoon, H.-K. Song, H.-W. Lee, M.-J. Cheng, Y. Kwon, Energy Environ. Sci. 2023, 16, 2003.
- [11] D.-S. Huang, X.-F. Qiu, J.-R. Huang, M. Mao, L. Liu, Y. Han, Z.-H. Zhao, P.-Q. Liao, X.-M. Chen, Nature Synthesis 2024, 3, 1404.
- [12] M. D. Zhang, J. R. Huang, P. Q. Liao, X. M. Chen, Chem Commun (Camb) 2024, 60, 3669.
- [13] Y. Cai, J. Fu, Y. Zhou, Y.-C. Chang, Q. Min, J.-J. Zhu, Y. Lin, W. Zhu, Nat. Commun. 2021, 12, 586.
- [14] X. Liu, P. V. Kumar, Q. Chen, L. Zhao, F. Ye, X. Ma, D. Liu, X. Chen, L. Dai, C. Hu, Appl. Catal., B 2022, 316, 121618.
- [15] X. Fan, C. Liu, X. He, Z. Li, L. Yue, W. Zhao, J. Li, Y. Wang, T. Li, Y. Luo, D. Zheng, S. Sun, Q. Liu, L. Li, W. Chu, F. Gong, B. Tang, Y. Yao, X. Sun, Adv. Mater. 2024, 36, 2401221.
- [16] X. Huang, Y. Li, S. Xie, Q. Zhao, B. Zhang, Z. Zhang, H. Sheng, J. Zhao, Angew. Chem., Int. Ed. 2024, 63, 202403980.
- [17] J. Leverett, T. Tran-Phu, J. A. Yuwono, P. Kumar, C. Kim, Q. Zhai, C. Han, J. Qu, J. Cairney, A. N. Simonov, R. K. Hocking, L. Dai, R. Daiyan, R. Amal, Adv. Energy Mater. 2022, 12, 2201500.
- [18] X.-F. Qiu, J.-R. Huang, C. Yu, X.-M. Chen, P.-Q. Liao, Angew. Chem., Int. Ed. 2024, n/a, 202410625.
- [19] H. Wan, X. Wang, L. Tan, M. Filippi, P. Strasser, J. Rossmeisl, A. Bagger, ACS Catal. 2023, 13, 1926.
- [20] H. Xiong, P. Yu, K. Chen, S. Lu, Q. Hu, T. Cheng, B. Xu, Q. Lu, Nat. Catal. 2024, 7, 785.
- [21] W. Chen, X. Yang, Z. Chen, Z. Ou, J. Hu, Y. Xu, Y. Li, X. Ren, S. Ye, J. Qiu, J. Liu, Q. Zhang, Adv. Funct. Mater. 2023, 33, 2300512.
- [22] L. Liu, T. Xiao, H. Fu, Z. Chen, X. Qu, S. Zheng, Appl. Catal., B 2023, 323, 122181.
- [23] S. Zhang, J. Wu, M. Zheng, X. Jin, Z. Shen, Z. Li, Y. Wang, Q. Wang, X. Wang, H. Wei, J. Zhang, P. Wang, S. Zhang, L. Yu, L. Dong, Q. Zhu, H. Zhang, J. Lu, Nat. Commun. 2023, 14, 3634.
- [24] W.-D. Zhang, H. Dong, L. Zhou, H. Xu, H.-R. Wang, X. Yan, Y. Jiang, J. Zhang, Z.-G. Gu, Appl. Catal., B 2022, 317, 121750.
- [25] Z. Li, M. Xu, J. Wang, Y. Zhang, W. Liu, X. Gu, Z.-K. Han, W. Ye, G. Li, Small **2024**, n/a, 2400036.
- [26] S. Cao, S. Zhou, H. Chen, S. Wei, S. Liu, X. Lin, X. Chen, Z. Wang, W. Guo, X. Lu, Energy & Environmental Materials 2022, 6,2102209.
- [27] Q. Ma, H. Jin, J. Zhu, Z. Li, H. Xu, B. Liu, Z. Zhang, J. Ma, S. Mu, Adv. Sci. 2021, 8, 2102209.
- [28] Y. Li, S. Zheng, H. Liu, Q. Xiong, H. Yi, H. Yang, Z. Mei, Q. Zhao, Z.-W. Yin, M. Huang, Y. Lin, W. Lai, S.-X. Dou, F. Pan, S. Li, Nat. Commun. 2024, 15, 176.
- [29] J. Graciani, K. Mudiyanselage, F. Xu, A. E. Baber, J. Evans, S. D. Senanayake, D. J. Stacchiola, P. Liu, J. Hrbek, J. F. Sanz, J. A. Rodriguez, Science 2014, 345, 546.
- [30] S. Kattel, P. Liu, J. G. Chen, J. Am. Chem. Soc. 2017, 139, 9739.
- [31] F. Li, Q. Huo, X. Zhou, S. Fang, F. Han, J. Yang, Q. Guan, W. Li, Applied Catalysis B: Environment and Energy 2025, 363, 124819.
- [32] J. A. Farmer, C. T. Campbell, Science 2010, 329, 933.
- [33] Q. Cheng, M. Huang, L. Xiao, S. Mou, X. Zhao, Y. Xie, G. Jiang, X. Jiang, F. Dong, ACS Catal. 2023, 13, 4021.
- [34] M. Muhyuddin, G. Zuccante, P. Mustarelli, J. Filippi, A. Lavacchi, L. Elbaz, Y.-H. Chen, P. Atanassov, C. Santoro, Energy Environ. Sci. 2024, 17, 3739.
- [35] Y. Yu, Y. Sun, J. Han, Y. Guan, H. Li, L. Wang, J. Lai, Energy Environ. Sci. 2024, 17, 5183.
- [36] H. Zhang, C. Wang, H. Luo, J. Chen, M. Kuang, J. Yang, Angew. Chem., Int. Ed. 2023, 62, 202217071.
- [37] J. Zhou, M. Wen, R. Huang, Q. Wu, Y. Luo, Y. Tian, G. Wei, Y. Fu, Energy Environ. Sci. 2023, 16, 2611.

- [38] M. Ferri, L. Delafontaine, S. Guo, T. Asset, P. Cristiani, S. Campisi, A. Gervasini, P. Atanassov, ACS Energy Lett. 2022, 7, 2304.
- [39] A. Tripathi, R. Thapa, Carbon 2023, 208, 330.
- [40] Y. Zhang, H. Zhou, Y. Zhang, Z. Shi, W. Xiong, L. Chen, W. Liu, H. Du, J. Xu, S. Chi, Y. Zhang, J. Kan, J. Dai, X. Xie, Applied Catalysis B: Environment and Energy 2024, 15, 124262.
- [41] G. Spezzati, A. D. Benavidez, A. T. DeLaRiva, Y. Su, J. P. Hofmann, S. Asahina, E. J. Olivier, J. H. Neethling, J. T. Miller, A. K. Datye, E. J. M. Hensen, Appl. Catal., B 2019, 243, 36.
- [42] H. Li, S. Ma, H. Cai, H. Zhou, Z. Huang, Z. Hou, J. Wu, W. Yang, H. Yi, C. Fu, Y. Kuang, Energy Storage Mater. 2019, 18, 338.
- [43] Y. Chu, Q. Ma, X. Hou, Y. Zhang, J. Zhang, X. Ni, Y. Wang, J. Cleaner Prod. 2023, 425, 139005.
- [44] T. Jia, L. Wang, Z. Zhu, B. Zhu, Y. Zhou, G. Zhu, M. Zhu, H. Tao, Chin. Chem. Lett. 2024, 35, 108692.
- [45] D. Yu, M. Wu, Q. Hu, L. Wang, C. Lv, L. Zhang, J. Hazard. Mater. 2019, 367, 456,
- [46] G. Wang, J. Zhang, S. Lin, H. Xiao, Q. Yang, S. Chen, B. Yan, Y. Gu, Cellulose 2019, 27, 2085.
- [47] Y.-t. Zhang, S.-y. Li, N.-n. Zhang, G. Lin, R.-q. Wang, M.-n. Yang, K.-k. Li, New Carbon Materials 2023, 38, 200.
- [48] S. Zhang, J. Wu, M. Zheng, X. Jin, Z. Shen, Z. Li, Y. Wang, Q. Wang, X. Wang, H. Wei, J. Zhang, P. Wang, S. Zhang, L. Yu, L. Dong, Q. Zhu, H. Zhang, J. Lu, Nat. Commun. 2023, 14,3634.
- [49] Y. Zhang, J. Yang, Z. Yu, Y. Hou, R. Jiang, J. Huang, F. Yang, S. Yao, L. Gao, W. Tang, Chem. Eng. J. 2021, 416, 129124.
- [50] S. B. Hassen, L. Bousselmi, P. Berçot, M. El Rezrazi, E. Triki, Rare Met.
- [51] Y. Zhang, X. Jia, G. Xu, W. Liu, D. Hu, Q. Sun, J. Xu, G. Zhang, W. Xiong, Z. Ma, Y. Zhang, J. Dai, H. zhou, D. Wu, X. Xie, Sep. Purif. Technol. 2023, 327, 124916.
- [52] Y. Zhang, J. Yang, Z. Yu, Y. Hou, R. Jiang, J. Huang, F. Yang, S. Yao, L. Gao, W. Tang, Chem. Eng. J. 2021, 416, 129124.
- [53] Y. Zhu, W. Zhao, J. Zhang, Z. An, X. Ma, Z. Zhang, Y. Jiang, L. Zheng, X. Shu, H. Song, X. Xiang, J. He, ACS Catal. 2020, 10,
- [54] M. Wang, G. Zhang, J. Zhu, W. Li, J. Wang, K. Bian, Y. Liu, F. Ding, C. Song, X. Guo, Chem. Eng. J. 2022, 446, 137212.
- [55] S. E. Mousavi Ghahfarokhi, E. Mohammadzadeh Shobegar, M. Zargar Shoushtari, J. Supercond. Novel Magn. 2018, 32, 1067.
- [56] M. Cong, Q. Liu, D. Wang, S. Hao, Z. Han, H. Xu, M. Guo, X. Ding, Y. Gao, Applied Catalysis B: Environment and Energy 2024, 351, 123941.
- [57] H. Fang, Z. Wang, C.-H. Kuo, H. Yang, X. Feng, W. Ji, C.-T. Au, Chem. Eng. J. 2024, 486, 150178.
- [58] Y. Gao, J. Wang, M. Sun, Y. Jing, L. Chen, Z. Liang, Y. Yang, C. Zhang, J. Yao, X. Wang, Angew. Chem., Int. Ed. 2024, 136, 202402215.
- [59] J. Geng, S. Ji, M. Jin, C. Zhang, M. Xu, G. Wang, C. Liang, H. Zhang, Angew. Chem., Int. Ed. 2023, 62, 202210958.
- [60] C. Lv, C. Lee, L. Zhong, H. Liu, J. Liu, L. Yang, C. Yan, W. Yu, H. H. Hng, Z. Qi, L. Song, S. Li, K. P. Loh, Q. Yan, G. Yu, ACS Nano 2022, 16, 8213.
- [61] M. Sun, G. Wu, J. Jiang, Y. Yang, A. Du, L. Dai, X. Mao, Q. Qin, Angew. Chem., Int. Ed. 2023, 62, 202301957.
- [62] X. Wei, X. Wen, Y. Liu, C. Chen, C. Xie, D. Wang, M. Qiu, N. He, P. Zhou, W. Chen, J. Cheng, H. Lin, J. Jia, X.-Z. Fu, S. Wang, J. Am. Chem. Soc. 2022, 144, 11530.
- [63] Y. Zhao, Y. Ding, W. Li, C. Liu, Y. Li, Z. Zhao, Y. Shan, F. Li, L. Sun, F. Li, Nat. Commun. 2023, 14, 4491.
- [64] M. Ma, J. Wang, Y. Bai, P. Lv, X. Song, W. Su, L. Ding, J. Wei, G. Yu, Fuel 2021, 301, 121064.
- M. H. R. Mesquita-Britto, M. C. P. Mendonça, E. S. Soares, K. K. [65] Sakane, M. A. da Cruz-Höfling, Neurochem. Int. 2018, 120, 64.
- X. Feng, S. Zhang, R. Liu, J. Ma, X. Xu, J. Xu, X. Fang, X. Wang, Phys. Chem. Chem. Phys. 2022, 24, 3250.



www.advancedsciencenews.com



www.afm-journal.de

16163028, 2025, 28, Downloaded from https://advanced.onlinelibrary.wiley.com/doi/10.1002/adfm.202423568 by Ajying wang - Ningbo Institute Of Materials

, Wiley Online Library on [09/10/2025]. See the Terms

and-conditions) on Wiley Online Library for rules of use; OA articles are governed by the applicable Creative Commons

- [67] R. L. Frost, K. L. Erickson, M. L. Weier, P. Leverett, P. A. Williams, Spectrochim. Acta, Part A 2005, 61, 607.
- [68] I. K. Barker, V. Fawcett, D. A. Long, J. Raman Spectrosc. 1987, 18, 71.
- [69] K. M. Khan, H. Krishna, S. K. Majumder, P. K. Gupta, Food Analytical Methods 2015, 8, 93.
- [70] Y. Gao, J. Wang, M. Sun, Y. Jing, L. Chen, Z. Liang, Y. Yang, C. Zhang, J. Yao, X. Wang, Angew. Chem., Int. Ed. 2024, 63, 202402215.
- [71] M. Yuan, J. Chen, H. Zhang, Q. Li, L. Zhou, C. Yang, R. Liu, Z. Liu, S. Zhang, G. Zhang, Energy Environ. Sci. 2022, 15, 2084.
- [72] K. Fan, W. Xie, J. Li, Y. Sun, P. Xu, Y. Tang, Z. Li, M. Shao, Nat. Commun. 2022, 13, 7958.
- [73] J. Hu, S. Osella, E. A. dos Reis, A. B. da Silva, C. Ribeiro, L. H. Mascaro, J. Albero, H. Garcia, Applied Catalysis B: Environment and Energy 2024, 357, 124247.
- [74] C. Lin, X. Chen, L. Wang, W. Li, Z. Wang, M. Li, J. Feng, B. Hou, W. Yan, Adv. Funct. Mater. 2024, 34, 2401287.
- [75] P. Li, Z. Jin, Z. Fang, G. Yu, Energy Environ. Sci. 2021, 14,
- [76] J. Long, S. Chen, Y. Zhang, C. Guo, X. Fu, D. Deng, J. Xiao, Angewandte Chemie International Edition 2020, 59, 9711.
- [77] Y. Wang, C. Wang, M. Li, Y. Yu, B. Zhang, Chem. Soc. Rev. 2021, 50,